Inorganic Chemistry

Article

pubs.acs.org/IC

Ancillary Ligand Effects upon Dithiolene Redox Noninnocence in Tungsten Bis(dithiolene) Complexes

Yong Yan,[†,#] Christopher Keating,[†] Perumalreddy Chandrasekaran,[⊥] Upul Jayarathne,[†,○] Joel T. Mague,[†] Serena DeBeer,[§,‡] Kyle M. Lancaster,[‡] Stephen Sproules,[∥] Igor V. Rubtsov,[†] and James P. Donahue*[,†]

[†]Department of Chemistry, Tulane University, 6400 Freret Street, New Orleans, Louisiana 70118-5698, United States

[⊥]Department of Chemistry and Biochemistry, Lamar University, Beaumont, Texas 77710, United States

[§]Max-Planck Institute for Chemical Energy Conversion, Stiftstrasse 34-36, D-45470, Mülheim an der Ruhr, Germany

[‡]Department of Chemistry and Chemical Biology, Baker Laboratory, Cornell University, Ithaca, New York 14853, United States

[∥]WestCHEM, School of Chemistry, University of Glasgow, Glasgow, G12 8QQ, United Kingdom

Supporting Information

ABSTRACT: An expanded set of compounds of the type $[W(S_2C_2Me_2)_2L_1L_2]^n$ (n = 0: L_1 = L_2 = CO, **1**; L_1 = L_2 = CN^{t}Bu, **2**; L_1 = CO, L_2 = carbene, **3**; L_1 = CO, L_2 = phosphine, **4**; L_1 = L_2 = phosphine, **5**. n = 2−: L_1 = L_2 = CN^-, $[\mathbf{6}]^{2-}$) has been synthesized and characterized. Despite isoelectronic formulations, the compound set reveals gradations in the dithiolene ligand redox level as revealed by intraligand bond lengths, $\upsilon_{CCchelate}$, and rising edge energies in the sulfur K-edge X-ray absorption spectra (XAS). Differences among the terminal series members, **1** and $[\mathbf{6}]^{2-}$, are comparable to differences seen in homoleptic dithiolene complexes related by full electron transfer to/from a dithiolene-based MO. The key feature governing these differences is the favorable energy of the CO π^* orbitals, which are suitably positioned to overlap with tungsten d orbitals and exert an oxidizing effect on both metal and dithiolene ligand via π-backbonding. The CN^- π^* orbitals are too high in energy to mix effectively with tungsten and thus leave the filled dithiolene π^* orbitals unperturbed. This work shows how, and the degree to which, the redox level of a noninnocent ligand can be modulated by the choice of ancillary ligands(s).

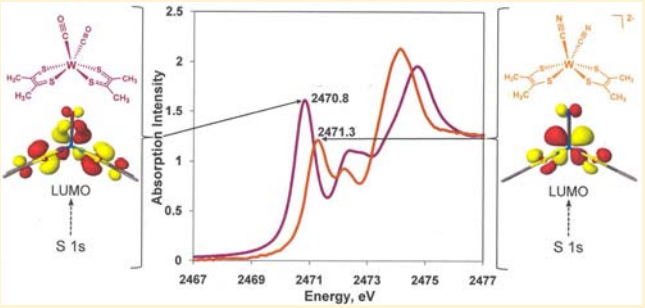

INTRODUCTION

Redox "noninnocent" behavior by a ligand can present complications in describing the electronic structures of its transition metal complexes but, to an ever increasing degree, is now appreciated as an aspect of coordination chemistry that can be definitively clarified with the combined insights afforded by spectroscopic data, X-ray crystallography, and computational analysis. A relatively recent trend is the deliberate incorporation of redox noninnocence into ligand design such that a supporting ligand itself serves as a source or sink of reducing equivalents,[1−4] thereby enabling reactivity with complexes of base metals that has traditionally been associated with noble metals.[5] The dithiolene ligand (Scheme 1) is a prototypical redox noninnocent ligand. For example, it was recognized in the 1970s that ligand reduction, rather than metal reduction, governs the series $[V(S_2C_2Ph_2)_3]^n$ (n = 0, 1−, 2−) on the basis that EPR spectra of the n = 0 and 2− members were essentially identical and consistent with a d^1 count at vanadium.[8] More recently, the power of sulfur K-edge X-ray absorption spectroscopy (XAS) to discern different levels of oxidation at sulfur has been used to show decisively that the redox processes involved in the series $[V(S_2C_2R_2)_3]^{0,1-,2-}$,[9] $[Re(S_2C_2Ph_2)_3]^{1+,0,1-}$,[10] $[Mo(bdt)_3]^{0,1-}$ (bdt = benzene-1,2-dithiolate(2-)),[11] $[Mo(S_2C_2Me_2)_3]^{0,1-,2-}$,[12] and $[Ni(S_2C_2Me_2)_2]^{0,1-,2-1}$[13] are all attributable to dithiolene ligand.

Scheme 1. (a−c) Dithiolene Ligand Redox States[a]

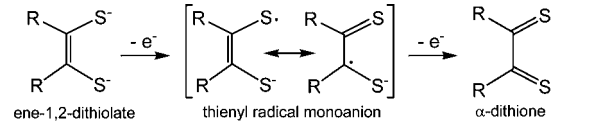

[a]Bond lengths are taken from the structures of $[Ni(S_2C_2Me_2)_2]^n$ (n = 2−, 0, for (a) and (b), respectively)[6] and $[Ni(Me_2pipdt)_2]^{2+}$[7] (Me_2pipdt = 1,4-dimethylpiperazine-2,3-dithione).

In the course of surveying general reactivity patterns of midvalent tungsten dithiolene complexes,[14] we have synthesized an expanded set of heteroleptic compounds of the general type $[W(S_2C_2Me_2)_2L_2]^n$ (L = CO, CNR, PR_3, carbene, CN^-; n = 0 or 2−). Although they exist ostensibly with the same formal

Received: April 13, 2013
Published: May 15, 2013

   dx.doi.org/10.1021/ic4009174 | Inorg. Chem. 2013, 52, 6743−6751

charge at tungsten, these complexes manifest variations in color that suggest fundamental differences in electronic structure. The study reported herein has revealed that changes in the dithiolene ligand redox level underpin these patent differences in electronic absorption spectra. Not only are these differences quantifiable by crystallography, but they are readily correlated to sulfur K-edge XAS data and to ligand $CC_{chelate}$ stretching frequencies in the resonance Raman spectra. At the extremes in this series of isoelectronic complexes, the differences in apparent dithiolene reduction are equivalent to changes observed upon full electron transfer in homoleptic dithiolene complexes in which the redox active MO is known to be dithiolene-based. Since the only parameter varied in this series is the nature and identity of the ancillary ligands L, this effect is referred to here as an "ancillary ligand effect" on dithiolene redox noninnocence.

That ancillary ligands, while "innocent," may play an important role in deciding the electronic structure of a redox-active ligand(s) coordinated to a transition metal is an aspect on the topic of noninnocent systems that is eliciting increasing notice. Switching between Fe^{II} and Fe^{III} attended by offsetting dithiolene redox chemistry has been noted in 5-coordinate $Fe(dithiolene)_2L$ complexes as a function of L.[15] Other examples include five-coordinate bis(imino)pyridine complexes of Mn that may be either Mn^{II} or Mn^{I} depending on whether the remaining two ligands are THF or CO, respectively,[16] and the observation of substantial changes in Ir-corrole covalency as a function of the natures of the axially bound pyridyl ligands.[17]

In conjunction with a fundamental interest in the interplay between metal and ligand in the electronic structure of these compounds, the practical consideration that ancillary ligands may exert a substantial tuning effect upon the redox behavior of a designed redox noninnocent ligand, and consequently the reactivity of its complex with a metal, motivates this research.

EXPERIMENTAL SECTION

Syntheses. The numbering system by which all compounds are hereafter identified is defined in Chart 1 and Scheme 2. The starting materials $[W(CO)_3(MeCN)_3]$[18] and $[Ni(mdt)_2]$[14] were synthesized according to literature procedures, as were compounds **1**,[14] **4a**,[14] **5a**,[14] **9**,[14] and $[Et_4N][W(S_2C_2Me_2)_3]$.[19] All other reagents were purchased from commercial sources and used as received. All solvents were purchased from either Pharmco-AAPER or Sigma-Aldrich. Solvents either were dried with a system of drying columns from the Glass Contour Company (CH_2Cl_2, THF, Et_2O, *n*-pentane, hexanes) or were freshly distilled prior to use according to standard literature procedures[20] and stored in a glovebox (^{t}BuOMe, MeCN, MeOH, 1,2-dichloroethane). Silica columns were run in the open air using 60-230 μm silica (Dynamic Adsorbents). All reactions were conducted under an atmosphere of either N_2 or Ar.

Chart 1. Compound Number Scheme

$[W(S_2C_2Me_2)_2(CO)_2]$	**1**
$[W(S_2C_2Me_2)_2(C{\equiv}N^tBu)_2]$	**2**
$[W(S_2C_2Me_2)_2(CO)(IMes)]$[a]	**3**
$[W(S_2C_2Me_2)_2(CO)(PMe_3)]$	**4a**
$[W(S_2C_2Me_2)_2(CO)(PMe_2Ph)]$	**4b**
$[W(S_2C_2Me_2)_2(CO)(PMePh_2)]$	**4c**
$[W(S_2C_2Me_2)_2(CO)(P^tBuPh_2)]$	**4d**
$[W(S_2C_2Me_2)_2(CO)(PPh_3)]$	**4e**
$[W(S_2C_2Me_2)_2(CO)(P(NMe_2)_3)]$	**4f**
$[W(S_2C_2Me_2)_2(PMe_3)_2]$	**5a**
$[W(S_2C_2Me_2)_2(PMe_2Ph)_2]$	**5b**
$[W(S_2C_2Me_2)_2(dppe)]$	**5c**
$[Et_4N]_2[W(S_2C_2Me_2)_2(CN)_2]$	$[Et_4N]_2$[**6**]
$[W(S_2C_2Me_2)(CO)_2(PMe_3)_2]$	**7a**
$[W(S_2C_2Me_2)(CO)_2(PMe_2Ph)_2]$	**7b**
$[W(S_2C_2Me_2)(CO)_2(PMePh_2)_2]$	**7c**
$[W(S_2C_2Me_2)(CO)_2(PPh_3)_2]$	**7d**
$[W(S_2C_2Me_2)(CO)_3(IMes)]$[a]	**8**
$[W(S_2C_2Me_2)(CO)_4]$	**9**

[a]IMes = 1,3-bis(2,4,6-trimethylphenyl)imidazol-2-ylidene.

$[W(S_2C_2Me_2)_2(CN^tBu)_2]$, ***2***. To a solution of **1** (0.20 g, 0.42 mmol) in CH_2Cl_2 (20 mL) was slowly added CN^tBu (0.25 mL, 0.18 g, 2.21 mmol) via syringe at ambient temperature. During the course of this addition, the evolution of gaseous CO was observed, and the color of the reaction mixture turned from magenta to a dark orange hue. Stirring was continued at room temperature for 4 h, whereupon the solvent was removed under reduced pressure to afford a dark orange solid residue, which was washed with *n*-pentane (2 × 5 mL) and dried overnight. Yield: 0.19 g, 0.32 mmol, 76%. ^{1}H NMR (δ, ppm in $CDCl_3$): 1.54 (s, 18H, $C(CH_3)_3$), 2.68 (s, 12H, dithiolene CH_3). IR (KBr, cm^{-1}): 2125 (vs, CN), 1520 (vs, C═C). Absorption spectrum (CH_2Cl_2) λ_{max} nm (ε_M): ~272 (sh, 29200), 367 (14400), 459 (15900), ~510 (sh, 11700). $[W(mdt)_2(CN^tBu)_2] + e^- \rightarrow [W(mdt)_2(CN^tBu)_2]^{1-}$, −1.25 V; $[W(mdt)_2(CN^tBu)_2]^{1-} + e^- \rightarrow [W(mdt)_2(CN^tBu)_2]^{2-}$, −1.59 V. MALDI MS: *m/e* $C_{18}H_{30}N_2S_4W$: 586.081, Observed: 586.022. Anal. Calcd for $C_{18}H_{30}N_2S_4W$: C, 36.86; H, 5.16; N, 4.78. Found: C, 37.09; H, 5.12; N, 4.81.

$[W(S_2C_2Me_2)_2(CO)(IMes)]$, ***3***. A CH_2Cl_2 solution of 1,3-bis(2,4,6-trimethylphenyl)imidazol-2-ylidene (IMes) (0.13 g, 0.42 mmol) was transferred via cannula to a solution of **1** (0.20 g, 0.42 mmol) in CH_2Cl_2 (10 mL) at ambient temperature. The resulting dark orange reaction mixture was stirred for 12 h at ambient temperature, whereupon the solvent was removed under reduced pressure, and the remaining solid was washed with hexanes (3 × 5 mL) and dried under a vacuum. Yield: 0.22 g, 0.29 mmol, 69%. ^{1}H NMR (δ, ppm in CD_2Cl_2): 2.03 (s, 12H, mesityl CH_3), 2.25 (s, 6H, mesityl CH_3), 2.40 (broad singlet, 12H, dithiolene CH_3), 6.71 (s, 4H, aromatic C−*H*), 6.92 (s, 2H, *CH*═*CH*). IR (KBr, cm^{-1}): 1929 (vs, CO), 1936 (vs, CO), 1519 (C═C, dithiolene). Absorption spectrum (CH_2Cl_2) λ_{max} nm (ε_M): 370 (15900), 465 (18900), 532 (sh, 8210). $[W(mdt)_2(CO)(IMes)] - e^- \rightarrow [W(mdt)_2(CO)(IMes)]^{1+}$, 0.67 V (qr); $[W(mdt)_2(CO)(IMes)] + e^- \rightarrow [W(mdt)_2(CO)(IMes)]^{1-}$, −1.43 V. (MALDI MS: *m/e* for $C_{30}H_{36}N_2OS_4W$: 752.122, observed: 724.156 (M-CO). Anal. Calcd for $C_{30}H_{36}N_2OS_4W$: C, 47.87; H, 4.82; N, 3.72. Found: C, 47.72; H, 4.82; N, 3.83.

$[W(S_2C_2Me_2)_2(CO)(PPhMe_2)]$, ***4b***. A 50 mL flask with magnetic stir bar was charged with **1** (0.406 g, 0.853 mmol) under an Ar atmosphere. Toluene (20 mL) was added, and the mixture was stirred for 10 min, whereupon PMe_2Ph (0.117 g, 0.853 mmol) in toluene (5 mL) was added via syringe. The resulting reaction mixture was stirred for 4 h at ambient temperature. The solvent was removed under reduced pressure, and the residue was washed with 3 × 5 mL of pentane and dried. Yield: 0.324 g, 0.552 mmol, 65%. ^{1}H NMR (δ, ppm in $CDCl_3$): 7.22−7.20 (m, 3H, Ph), 6.83−6.78 (m, 2H, Ph), 2.74 (s, 12H, Me), 2.11 (d, J_{PH} = 9.2 Hz, 6H, P*Me*$_2$Ph). ^{13}C NMR (δ, ppm in $CDCl_3$): δ 231.53 (s, CO), 155.20 (br s, C═C), 136.81 (s, Ph), 136.31 (s, Ph), 131.65 (s, Ph), 130.37 (s, Ph), 128.7 (s, Ph), 24.085 (s, Me), 20.27 (d, J_{PC} = 35.8 Hz, P*Me*$_2$Ph). ^{31}P NMR (δ, ppm in $CDCl_3$): δ 11.22 (s, J_{PW} = 220.7 Hz). IR (KBr, cm^{-1}): 2905 (w), 1936 (vs, CO), 1435 (m), 1290 (m), 1085 (m), 901 (vs), 736 (s), 485 (s). Anal. Calcd for $C_{17}H_{23}OPS_4W$: C, 34.81; H, 3.95; P, 5.28. Found: C, 34.87; H, 3.91; P, 5.40.

$[W(S_2C_2Me_2)_2(CO)(PMePh_2)]$, ***4c***. Solutions of **1** (0.345 g, 7.2 mmol) and $PMePh_2$ (0.269 mL, 0.290 g, 14.4 mmol) were separately prepared in toluene (30 and 10 mL, respectively). The phosphine solution was transferred to the stirring solution of the **1** via cannula, which induced an immediate color change from magenta to red. A reflux condenser was affixed to the reaction vessel, and the mixture was refluxed for 3 h, during which time the color assumed more of a reddish-orange aspect. The solvent was evaporated under reduced

dx.doi.org/10.1021/ic4009174 | Inorg. Chem. 2013, 52, 6743−6751

Scheme 2. Syntheses and Numbering System for Compounds[a]

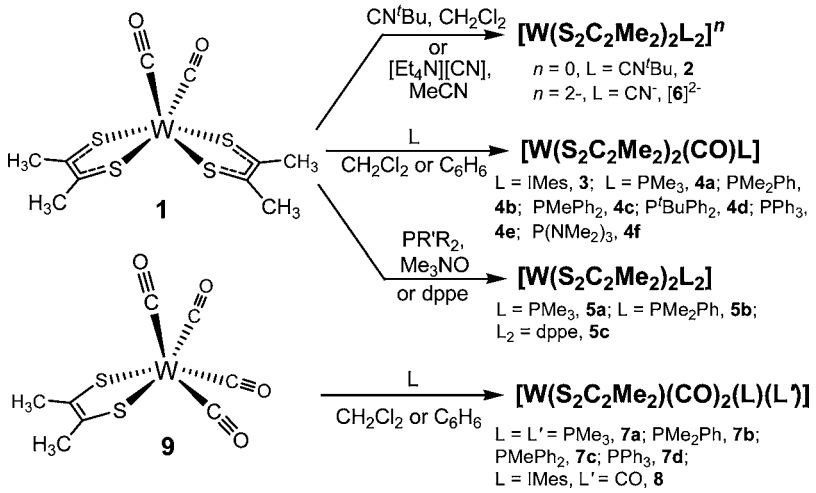

[a]IMes = 1,3-bis(2,4,6-trimethylphenyl)imidazol-2-ylidene.

pressure, and a reddish colored solid was obtained. This solid residue was purified on a silica column eluted with a mixture of CH_2Cl_2/hexanes (2:3). Complex **4c** was readily crystallized from the eluant as dark reddish-orange crystals. Yield: 0.292 g, 0.45 mmol, 62%. ^{31}P NMR (δ, ppm in C_6D_6): 26.17 (s, J_{PW} = 221 Hz). IR (KBr, υ in cm^{-1}): 1938 υ_{CO}. UV−vis (CH_2Cl_2), λ_{max} (ε_M): 482 (51500), 366 (27200). Anal. Calc. for $C_{22}H_{25}OPS_4W$: C, 40.75; H, 3.89; P, 4.78; S, 19.78. Found: C, 40.32; H, 3.78; P, 3.04; S, 19.90.

[W(S$_2$C$_2$Me$_2$)$_2$(CO)(P^{t}BuPh$_2$)], ***4d***. The procedure described for the synthesis and purification of **4c** was employed on a scale employing 0.200 g (0.42 mmol) of **1** and 0.101 g (0.42 mmol) of P^{t}BuPh$_2$. Complex **4d** readily crystallized from the chromatography eluant as dark red column-shaped crystals. Yield: 0.185 g, 0.254 mmol, 61%. IR (KBr, υ in cm^{-1}): 1936 υ_{CO}. MALDI MS: *m/e* for $C_{25}H_{31}OPS_4W$: 690.5983; observed: 661.838 (M-CO)$^+$, 419.604 (M-CO-P^{t}BuPh$_2$)$^+$. Anal. Calc. for $C_{25}H_{31}OPS_4W$: C, 43.48; H, 4.52; P, 4.49. Found: C, 43.79; H, 4.51; P, 4.35.

[W(S$_2$C$_2$Me$_2$)$_2$(CO)(PPh$_3$)], ***4e***. A Schlenk flask with stir bar was charged with portions of **1** (0.106 g, 0.223 mmol) and PPh_3 (0.117 g, 0.449 mmol) under a N_2 atmosphere. Freshly distilled benzene (15 mL) was added, and the mixture was heated to 85 °C with stirring for 12 h. After being cooled to room temperature, the solvent was removed from the reaction mixture under reduced pressure. The resulting crude product was purified on a silica chromatography column eluted first with hexanes to remove [W(S$_2$C$_2$Me$_2$)$_3$]. Continued elution with Et_2O enabled movement and collection of **4e** from the column. After evaporation of the eluant under reduced pressure and drying under a vacuum, **4e** was obtained as a dark orange product. Crystalline samples were prepared by the diffusion of *n*-pentane vapor into a solution in Et_2O. Yield: 0.129 g, 0.182 mmol, 81%. ^{1}H NMR (δ, ppm in $CDCl_3$): 7.28 (br s, 12H, Ph), 6.51 (br s, 3H, Ph), 2.72 (s, 12H, Me). ^{13}C NMR (δ, ppm in $CDCl_3$, 25 °C): 230.62 (CO), 156.18 (C═C), 135.21 (s, Ph), 135.12 (s, Ph), 130.60 (s, Ph), 128.53 (s, Ph), 128.43 (s, Ph), 24.15 (s, CH_3). ^{31}P NMR (δ, ppm in CD_2Cl_2): 39.58 (s, J_{PW} = 222.4 Hz). IR (KBr, cm^{-1}): 2909 (w), 1949 (vs, CO), 1432 (m), 1090 (s), 927 (w), 743 (m). Anal. Calcd for $C_{27}H_{27}OPS_4W$: C, 45.64; H, 3.83. Found: C, 45.80; H, 3.79.

[W(S$_2$C$_2$Me$_2$)$_2$(CO)(P(NMe$_2$)$_3$)], ***4f***. The procedure executed for the synthesis of **4f** was similar to that described for **4b**. The reaction scale involved 0.100 g (0.21 mmol) of **1** and excess P(NMe$_2$)$_3$ (0.120 mL, 0.66 mmol). Compound **4f** was obtained as red plate crystals by the diffusion of *n*-pentane vapor into a CH_2Cl_2-Et_2O solution. Yield: 0.015 g, 0.025 mmol, 12%. ^{1}H NMR (δ, ppm in CD_2Cl_2): 2.26 (very broad, 18H, (P(N(CH_3)$_2$)$_3$), 2.65 (s, 12H, dithiolene CH_3) Absorption spectrum (CH_2Cl_2) λ_{max} nm (ε_M): 356 (14700), 481 (16200). MALDI MS: *m/e* for $C_{15}H_{30}N_3OPS_4W$: 611.052, observed: 567.220 (M-CO-Me).

[W(S$_2$C$_2$Me$_2$)$_2$(dppe)], ***5c***. A 100 mL Schlenk flask with stir bar was charged with **1** (0.200 g, 0.42 mmol) and toluene (30 mL), while a solution of dppe (0.167 g, 0.42 mmol) in 10 mL of toluene was prepared in a separate flask. The dppe solution was transferred to that of **1**, which induced an immediate color change from magenta to red. A reflux condenser was fitted to this reaction flask, and the mixture was refluxed for 3 h, during which time the color turned to dark red. The solvent was evaporated under reduced pressure, and a reddish-colored solid was obtained. This solid residue was purified on a silica column eluted with a mixture of CH_2Cl_2/hexanes (1:4). Complex **5c** was recrystallized by diffusion of pentane vapor into a concentrated solution in benzene. Yield: 0.180 g, 0.220 mmol, 52%. MALDI MS: *m/e* for $C_{34}H_{36}P_2S_4W$: 818.6972, observed: 818.856 (M$^+$). Anal. Calcd for $[W(S_2C_2Me_2)_2(dppe)]\cdot{}^5/_6C_6H_6$, $C_{39}H_{41}P_2S_4W$: C, 53.00; H, 4.67; P, 7.01. Found: C, 53.02; H, 4.82; P, 6.73.

[Et$_4$N]$_2$[W(S$_2$C$_2$Me$_2$)$_2$(CN)$_2$], *[Et$_4$N]$_2$**[6]***. A 50 mL Schlenk flask under N_2 was charged with **1** (0.100 g, 0.21 mmol) and 20 mL of dry dichloromethane added via syringe. Under outward nitrogen flow, [Et$_4$N][CN] (0.066 g, 0.42 mmol) was added in one portion to the solution in the flask. Vigorous evolution of bubbles and a color change from reddish purple to orange were observed immediately. The resulting reaction mixture was stirred for another 2 h, and the solvent was then removed under reduced pressure. The residue was washed with diethyl ether (3 × 10 mL). Orange, block-shaped crystals that were suitable for X-ray diffraction were grown by diffusion of *tert*-butyl methyl ether into an acetonitrile solution. Yield: 0.098 g, 0.120 mmol, 57%. ^{1}H NMR (δ, ppm in CD_2Cl_2): 1.16 (t, 24H, NCH$_2$$CH_3$), 2.51 (s, 12H, dithiolene CH_3), 3.05 (q, 16H, NCH_2CH$_3$). IR (KBr, cm^{-1}): 2081 (vs, CN), 1556 (weak, dithiolene C═C symmetric), 1480 (strong, C═C, asymmetric), 1458 (strong, C═C, asymmetric). Absorption spectrum (CH_2Cl_2) λ_{max} nm (ε_M): 383 (34800), ~404 (sh, 33100), 494 (17200). $[W(mdt)_2(CN)_2]^{2-}$ + e$^-$ → $[W(mdt)_2(CN)_2]^{3-}$, −1.25 V; $[W(mdt)_2(CN)_2]^{3-}$ + e− → $[W(mdt)_2(CN)_2]^{4-}$, −1.85 V. Anal. Calcd for $C_{30}H_{58}N_6S_4W$: C, 44.22; H, 7.17; N, 10.31. Found: C, 44.13; H, 6.96; N, 10.16.

[W(S$_2$C$_2$Me$_2$)(CO)$_2$(PPhMe$_2$)$_2$], ***7b***. A 50 mL Schlenk flask with magnetic stir bar was charged with **9** (0.052 g, 0.127 mmol), PMe_2Ph (0.035 g, 0.255 mmol), and 10 mL of toluene. The reaction mixture was refluxed for 4 h, whereupon the solvent was removed under reduced pressure. The dark orange solid residue was washed with *n*-pentane and dried under a vacuum for 24 h. Yield: 0.058 g, 0.091 mmol, 73%. ^{1}H NMR (δ, ppm in $CDCl_3$): δ 7.24−7.22 (m, 6H, Ph), 7.14−7.09 (m, 4H, Ph), 2.53 (s, 6H, Me), 2.12 (d, J_{PH} = 9.6 Hz, 12H, PMe_2Ph). ^{31}P NMR (δ, ppm in $CDCl_3$): δ 6.41 (s, J_{PW} = 183.66 Hz). IR (KBr, cm^{-1}): 2965 (w), 1924 (vs, CO), 1826 (vs, CO), 1433 (m), 1256 (m), 1086 (s), 1021 (s), 909 (s), 792 (m), 698 (m).

dx.doi.org/10.1021/ic4009174 | *Inorg. Chem.* 2013, 52, 6743−6751

Table 1. Unit Cell and Refinement Data for Compounds 2, 3, 4cdef, 5bc, $[Et_4N]_2[6]$, 7bcd, 8, $[Et_4N][W(S_2C_2Me_2)_3]$

compound	2	3	4c	4d	4e
solvent	none	none	none	none	none
formula	$C_{18}H_{30}N_2S_4W$	$C_{30}H_{36}N_2OS_4W$	$C_{22}H_{25}OPS_4W$	$C_{25}H_{31}OPS_4W$	$C_{27}H_{27}OPS_4W$
fw	586.53	752.70	648.48	690.56	710.55
xtl system	monoclinic	monoclinic	monoclinic	monoclinic	triclinic
space grp	$P2_1/n$	$P2_1/c$	$P2_1$	$P2_1/n$	$P\bar{1}$
color, habit	red slat	red column	orange plate	red plate	brown block
a, Å	15.7588(16)	12.991(3)	10.323(3)	9.4584(7)	9.878(3)
b, Å	8.8549(9)	14.996(3)	9.456(3)	16.915(1)	10.203(3)
c, Å	17.5588(18)	15.949(4)	13.370(4)	16.942(1)	14.082(4)
α, deg	90	90	90	90	79.445(4)
β, deg	106.355(1)	98.188(3)	110.902(4)	99.637(1)	81.466(4)
γ, deg	90	90	90	90	78.219(3)
V, Å^3	2351.1(4)	3075.4(12)	1219.2(6)	2672.2(4)	1356.7(7)
T, K	100	100	100	100	100
Z	4	4	2	4	2
R_1, wR_2	0.0302, 0.0729	0.0212, 0.0494	0.0167, 0.0413	0.0211, 0.0431	0.0251, 0.0653
GOF	1.026	1.035	0.807	1.072	1.060
compound	4f	5b	5c	$[Et_4N]_2[6]$	7b
solvent	none	none	$1.5C_6H_6$	2MeCN	none
formula	$C_{15}H_{30}N_3OPS_4W$	$C_{24}H_{34}P_2S_4W$	$C_{43}H_{45}P_2S_4W$	$C_{30}H_{58}N_6S_4W$	$C_{22}H_{28}O_2P_2S_2W$
fw	611.48	696.54	935.82	814.91	634.35
xtl system	monoclinic	monoclinic	monoclinic	triclinic	monoclinic
space grp	$C2/c$	$P2_1/c$	$P2_1/n$	$P\bar{1}$	$P2_1/n$
color, habit	red plate	yellow plate	red plate	orange block	orange plate
a, Å	27.292(6)	19.413(4)	14.3288(7)	9.431(3)	9.516(4)
b, Å	9.699(2)	9.0400(17)	16.5017(8)	13.622(5)	15.328(6)
c, Å	17.754(4)	15.947(3)	17.5022(9)	15.748(6)	16.853(7)
α, deg	90	90	90	99.509(5)	90
β, deg	101.431(3)	104.240(2)	99.2550(10)	92.373(5)	97.849(7)
γ, deg	90	90	90	109.995(5)	90
V, Å^3	4606.4(16)	2712.7(9)	4084.5(4)	1864.6(11)	2435.0(16)
T, K	100	100	150	100	100
Z	8	4	4	2	4
R_1, wR_2	0.0250, 0.0491	0.0260, 0.0491	0.0329, 0.0712	0.0503, 0.1316	0.0182, 0.0436
GOF	1.061	1.026	1.071	1.048	1.041

compound	7c	7d	8	$[Et_4N][W(S_2C_2Me_2)_3]$
solvent	none	none	none	$1/2C_6H_6$
formula	$C_{32}H_{32}O_2P_2S_2W$	$C_{42}H_{36}O_2P_2S_2W$	$C_{28}H_{30}N_2O_3S_2W$	$C_{23}H_{41}NS_6W$
fw	758.49	882.62	690.51	707.78
xtl system	monoclinic	monoclinic	triclinic	monoclinic
space grp	$P2_1/n$	$P2_1$	$P\bar{1}$	$P2_1/n$
color, habit	orange parallelpiped	orange plate	brown slab	blue plate
a, Å	14.6817(7)	18.5335(13)	8.1260(15)	9.5750(11)
b, Å	11.2860(5)	9.9638(10)	9.2813(17)	24.536(3)
c, Å	19.6091(9)	21.866(3)	18.779(3)	12.7760(15)
α, deg	90	90	81.487(2)	90
β, deg	107.800(1)	114.207(9)	83.283(2)	106.042(1)
γ, deg	90	90	81.982(2)	90
V, Å^3	3093.6(2)	3682.9(6)	1380.3(4)	2884.6(6)
T, K	100	100	100	100
Z	4	4	2	4
R_1,[a,b] wR_2[b,c]	0.0282, 0.0546	0.0377, 0.0911	0.0209, 0.0511	0.0434, 0.0773
GOF[d]	1.191	1.062	1.070	1.046

[a] $R_1 = \Sigma||F_o| - |F_c||/\Sigma|F_o|$. [b] R indices for data cut off at $I > 2\sigma(I)$. [c] $wR_2 = \{[\Sigma w(F_o^2 - F_c^2)^2/\Sigma w(F_o^2)^2\}^{1/2}$; $w = 1/[\sigma^2(F_o^2) + (xP)^2 + yP]$, where $P = (F_o^2 + 2F_c^2)/3$. [d] GOF $= \{\Sigma[w(F_o^2 - F_c^2)^2]/(n - p)\}^{1/2}$, where n = number of reflections and p is the total number of parameters refined.

[W(S$_2$C$_2$Me$_2$)(CO)$_3$(IMes)], ***8.*** The procedure employed was analogous to that described for the synthesis of compound **3**. The scale employed for the reaction involved 0.050 g (0.12 mmol) of **9** and excess IMes (0.120 g, 0.39 mmol). Crystallization of **8** as brown, slab-shaped crystals was effected by diffusion of hexanes into a 1,2-dichloroethane solution. Yield: 0.041 g, 0.059 mmol, 49%. ^{1}H NMR (δ, ppm in CD_2Cl_2): 1.95 (s, 12H, mesityl CH_3), 2.25 (s, 6H, mesityl CH_3), 2.31 (s, 6H, dithiolene CH_3), 6.80 (s, 2H carbene $CH{=}CH$),

dx.doi.org/10.1021/ic4009174 | Inorg. Chem. 2013, 52, 6743−6751

7.00 (s, 4H, aromatic C−*H*). IR (KBr, cm^{-1}): 1992 (vs, CO), 1907 (vs, CO), 1884 (vs, CO), 1859 (s, CO), 1562 (m), 1481 (m), 612 (m). Absorption spectrum (CH_2Cl_2) λ_{max} nm (ε_M): ∼362 (sh, 15500), 433 (16800), ∼597 (sh, 4530). $[W(mdt)(CO)_3(IMes)] - e^- \rightarrow [W(mdt)(CO)_3(IMes)]^{1+}$, −0.74 V (ir); $[W(mdt)(CO)_3(IMes)] + e^- \rightarrow [W(mdt)(CO)_3(IMes)]^{1-}$, −1.16 V (qr). MALDI MS: *m*/*e* $C_{28}H_{30}O_3N_2S_2W$: 690.121, observed: 635.372 (M-2CO), 606.097 (M-3CO).

Physical Methods. All Raman spectra were acquired with a Nexus FT-Raman module with a 1064 nm excitation wavelength. All samples were prepared by smearing a solid sample of the complex onto paper, which then was mounted onto a magnetic plate placed in the focus of the laser. To reduce the absorbance background and avoid photobleaching, spectra were collected at a laser power ranging from 25 mW to 300 mW. The spectra presented are an average of 3000 scans, which subsequently improved the signal-to-noise ratio. Electronic absorption spectra were obtained at ambient temperature with a Hewlett-Packard 8452A diode array spectrophotometer, while IR spectra were taken as pressed KBr pellets with a Thermo Nicolet Nexus 670 FTIR instrument in absorption mode. All NMR spectra were recorded at 25 °C with a Varian Unity Inova spectrometer operating at 400, 100.5, or 161.8 MHz for ^1H, ^{13}C, and ^{31}P, respectively, and referenced to the solvent residual. Electrochemical measurements were obtained with a CHI620C electroanalyzer workstation using a Ag/AgCl reference electrode, a platinum disk working electrode, Pt wire as auxiliary electrode, and $[^nBu_4N][PF_6]$ as the supporting electrolyte. Under these conditions, the $[Cp_2Fe]^+/Cp_2Fe$ couple consistently occurred at +540 mV. X-ray absorption spectra were measured at the Stanford Synchrotron Radiation Lightsource (SSRL) under ring conditions of 3.0 GeV and 60−100 mA. Sulfur K-edge data were obtained using the 20-pole wiggler beamline 4-3 and 54-pole wiggler beamline 6-2. Tungsten L-edge spectra were measured on the 20-pole wiggler beamline 7-3, as previously described.[21] Elemental analyses were performed by Midwest Microlab, LLC of Indianapolis, IN, or by Canadian Microanalytical of Delta, British Columbia. Descriptions of the procedures for collection of X-ray diffraction data, the solution and refinement of crystal structures, and all computational details are deferred to Supporting Information.

RESULTS AND DISCUSSION

The synthesis of $[W(S_2C_2Me_2)_2L_2]^n$ (L = ^{t}BuNC, *n* = 0, **2**; L = CN^-, *n* = 2−, $[\mathbf{6}]^{2-}$) readily proceeds by straightforward ligand substitution from $[W(S_2C_2Me_2)_2(CO)_2]$ (**1**), the preparation of which was initially described by Schrauzer[22] but materially improved by Holm and Goddard[23] (Scheme 2). The analogous bis(phosphine) complexes, except that with dppe, require elevated temperatures and the use of Me_3NO as facilitating oxidant for the liberation of CO as CO_2. An enhanced W−CO backbonding interaction following substitution with a single phosphine ligand apparently necessitates forcing conditions for displacement of the second CO ligand. The π-acidic nature of both CN^tBu and CN^-, in contrast, appears to render the CO ligand quite labile toward substitution in the presumed monocarbonyl intermediates, $[W(S_2C_2Me_2)_2(CO)(CN^tBu)]$ and $[W(S_2C_2Me_2)_2(CO)(CN)]^{1-}$, which were not isolable.

The monocarbonyl compounds $[W(S_2C_2Me_2)_2(CO)L]$ (L = PR_3, carbene) form immediately with 1 equiv of L, excess L alone being ineffective in producing further substitution. All compounds occur nominally at the same total redox level and differ only in the character of the non-dithiolene ligands. A more limited set of compounds of the type $[W(S_2C_2Me_2)(CO)_2LL']$ (L = L′ = phosphine, **7**; L = carbene, L′ = CO, **8**) has been prepared from $[W(S_2C_2Me_2)(CO)_4]$ and is included.

With the exception of **4b**, all the compounds in Chart 1 have been structurally identified in this work or previously.[14,24,25] Unit cell, refinement data, and other crystallographic data are summarized in Table 1. All the bis(dithiolene) $[W(S_2C_2Me_2)_2L_2]^n$ compounds are trigonal prismatic with non-dithiolene ligands arranged is *cis* configuration along one of the long edges of a rectangular face. Gross structural features, such as Bailar twist angles and dihedral angles between dithiolene ligands, are typical of such complexes (Table S2). Thermal ellipsoid plots of **3** and $[\mathbf{6}]^{2-}$ suffice to represent all the bis(dithiolene) complexes (Figure 1). What is noteworthy

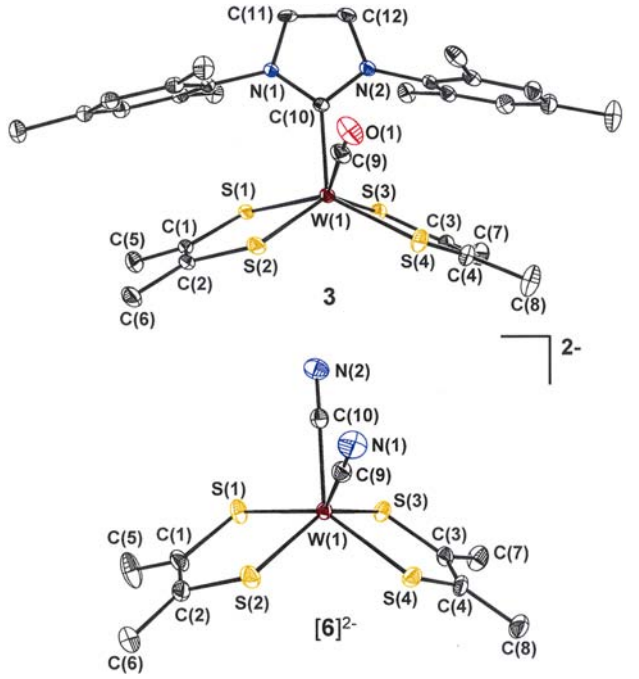

Figure 1. Thermal ellipsoid plots at the 50% probability level for **3** (top) and $[\mathbf{6}]^{2-}$ (bottom). Hydrogen atoms are omitted for clarity.

about the bis(dithiolene) compounds, when considered as a set, are dithiolene SC and $CC_{chelate}$ interatomic distances (Table 2) that increase and decrease, respectively, as the table is traversed from top toward bottom. Although juxtaposed pairs of compounds in the table do not have SC and $CC_{chelate}$ distances with uncertainties that meet the 3σ criterion that is indicative of a statistically significant difference,[26] **1** and $[\mathbf{6}]^{2-}$, which define the two extremes in this set of bis(dithiolene) compounds, do have meaningfully different SC bond lengths. These distances inversely correlate with the $CC_{chelate}$ bond lengths in a linear fashion (Figure S1) and are indicative of the redox level of the dithiolene ligand. Scheme 1 summarizes the canonical forms of the dithiolene ligand with corresponding intraligand bond lengths. With reference to the values in Scheme 1, the data in Table 2 imply radical monoanionic ligands in **1** and fully reduced ene-1,2-dithiolate dianions in $[\mathbf{6}]^{2-}$. The conclusion that emerges from the metric parameters in Table 2 is that the variable non-dithiolene ligands, referred to hereafter as the "ancillary" ligands, exert an important effect upon the redox state of the dithiolene ligand, and possibly the tungsten atom as well, even though all compounds exist with a metallodithiolene fragment that may be described with a common charge formalism. A similar situation likely pertains to the related mono(dithiolene) compounds **7**−**9**, but a suitably broad set of compounds with discernible structural differences is unavailable.

dx.doi.org/10.1021/ic4009174 | *Inorg. Chem.* 2013, 52, 6743−6751

Table 2. Dithiolene Redox Level in W Bis(dithiolene) Compounds Gauged by Crystallographic and Spectroscopic Markers

	bond lengths, Å[a]		sulfur K-edge XAS			$\upsilon_{CC\ chelate}$, cm^{-1}	
	SC	$CC_{chelate}$	pre-edge (eV)	α^2, LUMO[b]	edge (eV)[c]	Raman[d]	infrared[d]
1	1.722[2]	1.363[3]	2470.8, 2472.4	67	2474.2	1491.5 (18.1), 1476.0 (4.0)	1470.6
2	1.732[2]	1.360[4]	2471.1, 2472.4	57	2473.9	1523.7	1520.5
3	1.733[1]	1.354[2]				1523.1	1522.1
4a[14]	1.733[1]	1.354[2]	2471.0, 2472.3	54	2474.0	1515.5	1511.5
5a[14]	1.743[1]	1.346[2]	2471.2, 2472.2	46	2473.8	1555.7 (10.4), 1539.0 (4.8)	1553.3 (0.4), 1538.9 (1.1)
$[\mathbf{6}]^{2-}$	1.753[3]	1.339[6]	2471.3, 2472.3	48	2473.4	1556.8	1557.0
$[W(S_2C_2Me_2)_3]$[14]	1.74[1]	1.37[1]			2473.9	1487.0 (6.0), 1458.9 (25.0)	
$[W(S_2C_2Me_2)_3]^{1-}$	1.743[3]	1.354[5]			2473.4		
$[W(S_2C_2Me_2)_3]^{2-}$[20]	1.763[1]	1.337[2]					
7a[14]	1.754[4]	1.349(3)					
8	1.736[3]	1.348(4)					
9[14,21]	1.744[4]	1.351(8)			2473.4		

[a]Uncertainties in averaged bond lengths were determined using the general formula for uncertainty in a function of multiple variables as detailed by Taylor, J. R. *An Introduction to Error Analysis*; University Science Books: Sausalito, California, 1997; pp 73–77. [b]α^2 = covalency expressed as %. [c]Defined as the inflection point in the rising edge, determined from the second derivative of the intensity vs energy plot. [d]Two peaks visible owing to symmetric and asymmetric stretches; parenthetical values are relative intensities in arbitrary units.

The varying levels of dithiolene ligand reduction indicated by the structural data in Table 2 have been probed by sulfur K-edge X-ray absorption spectroscopy (XAS). This method involves transitions of core 1s electrons of sulfur to acceptor MOs with a degree of sulfur p character and, at high enough energy, their promotion into the continuum. The energy at which the latter excitation occurs directly correlates with Z_{eff} at sulfur and thereby can distinguish between reduced thiolate-type sulfur and an oxidized radical-type sulfur[27] (Scheme 1, panels a and b, respectively). The sulfur K-edge XAS for **1** and $[\mathbf{6}]^{2-}$ are overlaid in Figure 2, and their rising edge energies as well as those of other representative compounds from the set are presented in Table 2. The rising edge energy for **1** is 0.8 eV higher in energy than that for $[\mathbf{6}]^{2-}$, which accords with a higher Z_{eff} arising from its diminished thiolate character. This difference is comparable to the rising edge energy change (~0.5 eV) observed in reducing $[W(S_2C_2Me_2)_3]$ to its corresponding monoanion (Table 2). By analogy to the related molybdenum system,[12] the reduction of $[W(S_2C_2Me_2)_3]$ to $[W(S_2C_2Me_2)_3]^{1-}$ involves the addition of an electron to an MO comprised equally of the three dithiolene ligands such that the remaining "hole" is distributed equally among six sulfur atoms. The magnitude of the reduction seen at the dithiolene sulfur atoms in going from **1** to $[\mathbf{6}]^{2-}$ is surprising in view of the ease with which both CO ligands in **1** are displaced by CN^-, which would seem to suggest negligible difference between the two ligands in the nature and degree of their interaction with tungsten.

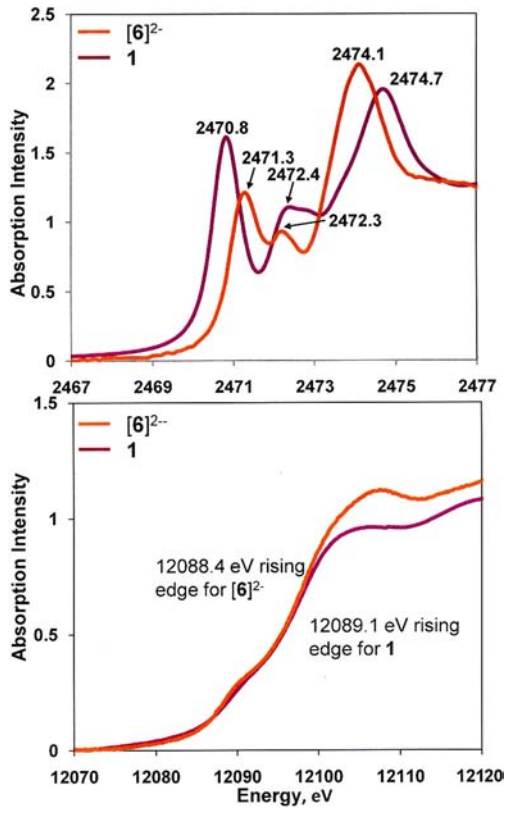

Figure 2. Sulfur K-edge (top), W L_1-edge XAS for **1**, $[\mathbf{6}]^{2-}$ (bottom).

The pre-edge features in the sulfur K-edge XAS of **1** and $[\mathbf{6}]^{2-}$ are also informative of the fundamental differences between them. The lowest energy absorption is assigned as a sulfur 1s → LUMO transition in these complexes as well as in **2**, **4a**, and **5a**. The intensity of these features correlates to the degree of sulfur p character in the composition of the LUMO, a greater contribution by the sulfur p orbitals being indicative of a higher degree of covalency (mixing) between metal and ligand. Deconvolution of the lowest energy features in the sulfur K-edge XAS from overlapping features (Figure S2), followed by integration of the absorption intensity (D_o), permits a quantitative assessment of the covalency (α^2) to the acceptor orbital via the relationship $D_o = (\alpha^2 h I_s)/3n$ (h = # holes in acceptor orbitals; I_s = radial transition dipole integral =14.22; n = # absorbing S atoms).[12] Expressed as percentages, covalencies for the LUMOs for **1**, **2**, **4a**, **5a**, and $[\mathbf{6}]^{2-}$ range from 67 to 46% (Tables 2 and S3). These values comport with the rising edge energies in showing that the fundamental difference between **1** and $[\mathbf{6}]^{2-}$ is greater ionic character (less covalency) to the latter, which is equivalent to saying that the dithiolene sulfur atoms in $[\mathbf{6}]^{2-}$ are more thiolate-like in nature.

The bond order changes implied by the variations in CS and $CC_{chelate}$ distances can be separately gauged by vibrational spectroscopy. The effectiveness of this technique in systems of this kind has been demonstrated by its use in identifying

dx.doi.org/10.1021/ic4009174 | Inorg. Chem. 2013, 52, 6743–6751

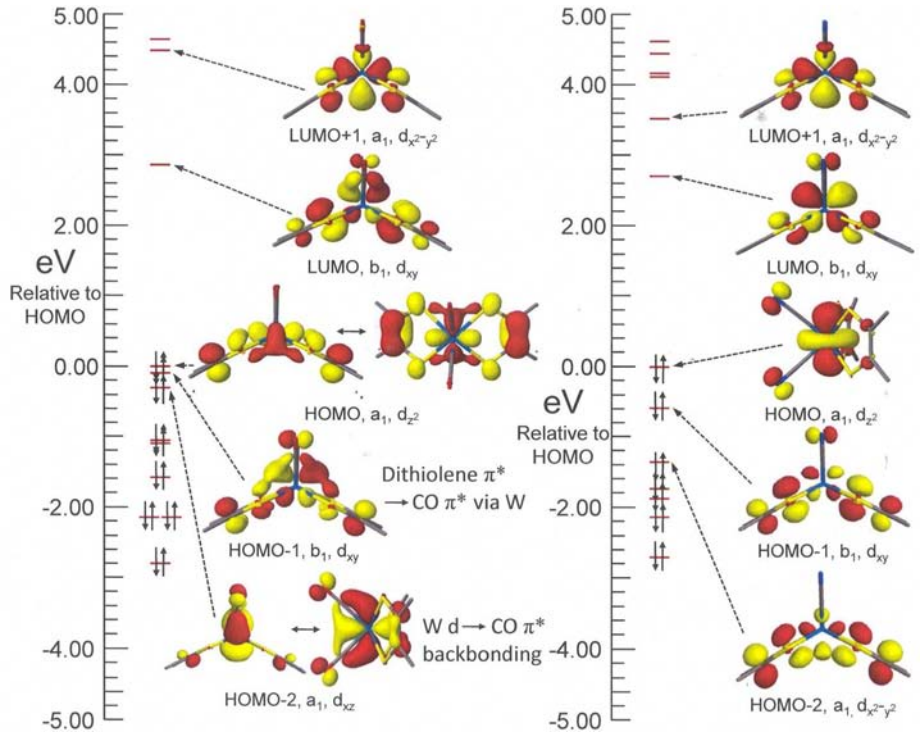

Figure 3. Comparison of the frontier MOs for **1** (left) and $[\mathbf{6}]^{2-}$ (right). The pseudo C_3 axis of the trigonal prism is taken as the z axis. Except for the HOMO of $[\mathbf{6}]^{2-}$, all orbital images (shown at the 0.05 contour level) are presented in the same relative orientation of the complexes.

dithiolene ligation to molybdenum in *R. sphaeroides* DMSO reductase.[28] The direct relationship between bond stretching frequency and interatomic force constant, and therefore interatomic bond order, provides independent but complementing insight into the ligand redox level. Here, symmetric CC bond stretching frequencies observed by Raman spectroscopy have been more accurately identified than their asymmetric modes in the IR, as the latter technique is complicated by the occurrence of strong interfering modes. Table 2 summarizes the SC and CC vibrational frequencies for compounds **1**-$[\mathbf{6}]^{2-}$, while Figure S3 presents a plot of υ_{CC} against the crystallographically determined $CC_{chelate}$ distances. The relationship is monotonic and, allowing for the uncertainties in the measurements, can be fit by a linear function.

As part of a DFT analysis of compounds **1**−**8**, Mulliken charges associated with the dithiolene ligand have been assessed and plotted against both the symmetric CC stretching frequencies and the rising edge energies in the sulfur K-edge X-ray absorption spectra (Figure S4). The linearity seen in these plots further affirms that these dithiolene ligand variations are real. With only one of the following values in hand − crystallographic $CC_{chelate}$ bond length, υ_{CC} from resonance Raman, rising edge energy in the sulfur K-edge XAS or computed Mulliken charge, the plots in Figures S3 and S4 provide a basis for estimating any of the remaining three.

A Mulliken population analysis of the frontier MOs in the optimized structures reveals changes in their composition that underpin the structural and spectroscopic data. Table S4 summarizes changes in the composition of the HOMO and LUMO, while Figure 3 illustrates these changes with orbital images for **1** and $[\mathbf{6}]^{2-}$, which are the terminal members of this series continuum and the two complexes that offer the clearest contrast. As noted by Holm and co-workers,[19] the frontier MOs for **1** are highly mixed between metal and ligands in a way that does not provide a straightforward d electron count at tungsten. Its HOMO is comprised of dithiolene π^* orbital and tungsten d orbital in a ∼64:21 ratio. The HOMO of $[\mathbf{6}]^{2-}$ differs sharply in being principally the d_{z^2} orbital (68%). The lower lying HOMO-1 and HOMO-2 of $[\mathbf{6}]^{2-}$ are similar to one another (Figure 3) and are primarily filled dithiolene π^* orbitals with modest metal character and therefore support the description of $[\mathbf{6}]^{2-}$ as a W^{IV} d^2 species. The LUMO for $[\mathbf{6}]^{2-}$ contrasts with that for **1** in having visibly less dithiolene π character (∼31% vs 62%) and proportionately more tungsten d character (49% vs 18%), a difference which is manifested in the lesser intensity of its first pre-edge feature in the sulfur K-edge XAS as compared to that of **1**.

Figure 3 reveals that the essential difference between **1** and $[\mathbf{6}]^{2-}$ is the suitable energy match, and therefore effective mixing, between the CO π^* orbitals and the tungsten d orbital manifold and π system of the dithiolene ligand, as compared to the CN^- π^* orbitals, which are too high in energy. The poor overlap between the CN^- π^* and tungsten d orbitals in the MO images for $[\mathbf{6}]^{2-}$ in Figure 3 is emphasized. In contrast to $[\mathbf{6}]^{2-}$, **1** has two filled MOs with significant W → CO π^* backbonding character. One of these is the HOMO-2, which effectively overlaps with the tungsten d_{xz}, draws electron density away from tungsten, and raises Z_{eff} at tungsten. Even more important to the understanding of **1** is the HOMO-1, which is comprised of filled dithiolene π^* orbitals and empty CO π^* orbitals interacting with the tungsten d_{xy} orbital. The consequence of this particular makeup is effective transfer of charge density from dithiolene to CO via tungsten, thereby oxidizing the dithiolene ligands in **1** as compared to $[\mathbf{6}]^{2-}$, as has been evidenced by several physical methods. A natural inclination is to presume that, if the dithiolene ligands are appreciably more oxidized in **1** than in $[\mathbf{6}]^{2-}$, then tungsten is commensurately

dx.doi.org/10.1021/ic4009174 | *Inorg. Chem.* 2013, 52, 6743−6751

more reduced. Importantly, Figure 3 shows that the relatively oxidized condition of the dithiolene ligands occurs *not at the expense of tungsten* but rather is *mediated by tungsten d orbitals and driven by the π-acidic nature of the CO ligands*. In support of this interpretation, Figure 2 presents an overlay of the tungsten L_1-edge X-ray absorption spectra for **1** and $[\mathbf{6}]^{2-}$ and shows a rising edge energy for **1** that is comparable to, even slightly *higher* in energy, than that for $[\mathbf{6}]^{2-}$. These values correlate directly with Z_{eff} at metal and indicate that, at least as this method can assess, the spectroscopic oxidation state of tungsten in both complexes is closer to W^{IV} than otherwise.

CONCLUSIONS

A principal conclusion arising from this study of isostructual, isoelectronic tungsten bis(dithiolene) complexes is that the ancillary ligands completing the coordination sphere can exert a significant effect upon the dithiolene redox level. This influence likely reflects the combination of ancillary ligand σ-donor strength with π-acidity, although the former is not as easily visualized as the latter in the orbital images of Figure 3. The variations seen in dithiolene redox level, which have been assessed structurally, spectroscopically, and computationally, are comparable in magnitude to the changes seen upon full electron transfer in homoleptic bis- and tris(dithiolene) complexes where the redox active orbital is dithiolene-based. Furthermore, the correlation between the data obtained by different methods provides a basis for gauging dithiolene CS or $CC_{chelate}$ bond distances, dithiolene υ_{CC}, sulfur K-edge XAS rising edge energy, or Mulliken charge for the dithiolene ligand if only one of the values is available. Our results demonstrate that the behavior of a redox noninnocent ligand engineered for a particular reactivity is subject, at least potentially, to considerable modulation by choice of ancillary ligand(s). More immediate to the present work is the observation that the $M(dithiolene)_2$ (M = Mo, W) fragment is common to a broad family of molybdenum and tungsten enzymes. Vibrational spectroscopy studies of *R. sphaeroides* DMSO reductase suggest differences in the redox level of the two pterin-dithiolene ligands in the enzyme's oxidized form, implying a degree of π-delocalization to one of them.[29] While the enzyme's redox chemistry is primarily Mo-based, partially oxidized dithiolene ligand may play a critical role in lowering the transition state energy during oxygen atom transfer from substrate to metal. Our results show that ancillary ligands with π orbitals of the right symmetry and energy (e.g., CO, possibly NO^+ or a suitably functionalized alkyne) have the capacity to effectively engage the π system of the dithiolene ligand(s) and render redox noninnocence operative.

ASSOCIATED CONTENT

Supporting Information

Full description of all procedures for crystal growth, diffraction data collection and processing, and structure solution and refinement; complete crystallographic data for all new structures in CIF format; thermal ellipsoid plots with complete atom labeling; S K-edge X-ray absorption spectra with first and second derivatives; description of basis sets employed and computational methods; *xyz* coordinates for optimized structures; supplementary figures as noted in text. This material is available free of charge via the Internet at http://pubs.acs.org.

AUTHOR INFORMATION

Corresponding Author

*E-mail: donahue@tulane.edu.

Present Addresses

[#](Y.Y.) Department of Chemistry, Princeton University, Princeton, New Jersey 08544.

[○](U.J.) Department of Chemistry, University of Illinois at Chicago, 845 West Taylor Street, MC 111, Chicago, Illinois, 60607.

Notes

The authors declare no competing financial interest.

ACKNOWLEDGMENTS

Support from NSF (Grant CHE-0845829 to J.P.D., Grant CHE-1012371 to I.V.R.), from DOE and NIH for support of the Stanford Synchrotron Radiation Lightsource at which portions of this research were conducted, from the Max Planck Society (SD), Cornell University (SD), the Sloan Foundation (SD), the Louisiana Board of Regents (Grant LEQSF-(2002-03)-ENH-TR-67) for the Tulane crystallography facility, and from IBM (fellowship support to Y.Y., C.K.) is gratefully acknowledged. Support from the EPSRC National UK EPR Facility and Service is gratefully acknowledged (S.S.).

REFERENCES

(1) Chirik, P. J. *Inorg. Chem.* **2011**, *50*, 9737−9740.
(2) Heyduk, A. F.; Zarkesh, R. A.; Nguyen, A. *Inorg. Chem.* **2011**, *50*, 9849−9863.
(3) Ouch, K.; Mashuta, M. S.; Grapperhaus, C. A. *Inorg. Chem.* **2011**, *50*, 9904−9914.
(4) Lippert, C. A.; Riener, K.; Soper, J. D. *Eur. J. Inorg. Chem.* **2012**, 554−561.
(5) Chirik, P. J.; Wieghardt, K. *Science* **2010**, *327*, 794−795.
(6) Lim, B. S.; Fomitchev, D. V.; Holm, R. H. *Inorg. Chem.* **2001**, *40*, 4257−4262.
(7) Bigoli, F.; Chen, C.-T.; Wu, W.-C.; Deplano, P.; Mercuri, M. L.; Pellinghelli, M. A.; Pilia, L.; Pintus, G.; Serpe, A.; Trogu, E. F. *Chem. Commun.* **2001**, 2246−2247.
(8) Kwik, W.-L.; Stiefel, E. I. *Inorg. Chem.* **1973**, *12*, 2337−2342.
(9) Sproules, S.; Weyhermüller, T.; DeBeer, S.; Wieghardt, K. *Inorg. Chem.* **2010**, *49*, 5241−5261.
(10) Sproules, S.; Weyhermüller, T.; Goddard, R.; Wieghardt, K. *Inorg. Chem.* **2011**, *50*, 12623−12631.
(11) Kapre, R. R.; Bothe, E.; Weyhermüller, T.; DeBeer George, S.; Wieghardt, K. *Inorg. Chem.* **2007**, *46*, 5642−5650.
(12) Tenderholt, A.; Szilagyi, R. K.; Holm, R. H.; Hodgson, K. O.; Hedman, B.; Solomon, E. I. *Inorg. Chem.* **2008**, *47*, 6382−6392.
(13) Szilagyi, R. K.; Lim, B. S.; Glaser, T.; Holm, R. H.; Hedman, B.; Hodgson, K. O.; Solomon, E. I. *J. Am. Chem. Soc.* **2003**, *125*, 9158−9169.
(14) Chandrasekaran, P.; Arumugam, K.; Jayarathne, U.; Pérez, L. M.; Mague, J. T.; Donahue, J. P. *Inorg. Chem.* **2009**, *48*, 2103−2113.
(15) Sproules, S.; Wieghardt, K. *Coord. Chem. Rev.* **2010**, *254*, 1358−1382.
(16) Russell, S. K.; Bowman, A. C.; Lobkovsky, E.; Wieghardt, K.; Chirik, P. J. *Eur. J. Inorg. Chem.* **2012**, 535−545.
(17) Palmer, J. H.; Lancaster, K. M. *Inorg. Chem.* **2012**, *51*, 12473−12482.
(18) Tate, D. P.; Knipple, W. R.; Augl, J. M. *Inorg. Chem.* **1962**, *1*, 433−434.
(19) Fomitchev, D. V.; Lim, B. S.; Holm, R. H. *Inorg. Chem.* **2001**, *40*, 645−654.
(20) Armarego, W. L. F.; Perrin, D. D. *Purification of Laboratory Chemicals*, 4th ed.; Butterworth-Heinemann: Oxford, Great Britain, 2000.

(21) Sproules, S.; Benedito, F. L.; Bill, E.; Weyhermüller, T.; DeBeer George, S.; Wieghardt, K. *Inorg. Chem.* **2009**, *48*, 10926−10941.
(22) Schrauzer, G. N.; Mayveg, V. P.; Heinrich, W. *J. Am. Chem. Soc.* **1966**, *88*, 5174−5179.
(23) Goddard, C. A.; Holm, R. H. *Inorg. Chem.* **1999**, *38*, 5389−5398.
(24) Sproules, S.; Banerjee, P.; Weyhermüller, T.; Yan, Y.; Donahue, J. P.; Wieghardt, K. *Inorg. Chem.* **2011**, *50*, 7106−7122.
(25) Yan, Y.; Chandrasekaran, P.; Mague, J. T.; DeBeer, S.; Sproules, S.; Donahue, J. P. *Inorg. Chem.* **2012**, *51*, 346−361.
(26) Stout, G. H.; Jensen, L. H. *X-Ray Structure Determination: A Practical Guide*; Wiley & Sons: New York, 1989; Chapter 18.
(27) Glaser, T.; Hedman, B.; Hodgson, K. O.; Solomon, E. I. *Acc. Chem. Res.* **2000**, *33*, 859−868.
(28) Gruber, S.; Kilpatrick, L.; Bastian, N. R.; Rajagopalan, K. V.; Spiro, T. G. *J. Am. Chem. Soc.* **1990**, *112*, 8179−8180.
(29) Johnson, M. K. *Prog. Inorg. Chem.* **2004**, *52*, 213−266.